Published in final edited form as:
Biomaterials. 2009 September ; 30(27): 4716–4722. doi:10.1016/j.biomaterials.2009.05.005.

The Artificial Peroxidase Activity of Magnetic Iron Oxide Nanoparticles and its Application to Glucose Detection

Faquan Yu[‡,#], **Yongzhuo Huang**[†,#], **Adam J. Cole**[#], and **Victor C. Yang**[†,#,*]

[†]Tianjin Key Laboratory of Modern Drug Delivery and High Efficiency, Tianjin University, Tianjin 300072, China

[‡]Key Laboratory for Green Chemical Process of Ministry of Education, Wuhan Institute of Technology, Wuhan 430073, China

[#]Department of Pharmaceutical Sciences, College of Pharmacy, University of Michigan, Ann Arbor, Michigan 48109, USA

Abstract

Aside from their superparamagnetic properties exploited in clinical magnetic resonance imaging (MRI), it was recently discovered that magnetic, iron oxide nanoparticles could function as an artificial, inorganic peroxidase. In this paper, we studied the impact of coating on the peroxidase activity of these nanoparticles. Nanoparticles with six different coating structures were synthesized and characterized by FTIR, TGA, TEM, size, zeta potential, and SQUID; and evaluated for peroxidase activity. Catalysis was found to follow Michaelis-Menten kinetics and peroxidase activity varied with respect to electrostatic affinity between nanoparticles and substrates, evidenced by differences in determined kinetic parameters. Glucose detection was selected as a model system because glucose could be indirectly measured from the release of hydrogen peroxide after its oxidation. Nanoparticles with high peroxidase activity exhibited higher sensitivity toward glucose, showing a larger linear slope when compared with those of low activity. A significantly improved linear correlation and detection limit of measured glucose could be readily obtained by manipulating the nanoparticle coating. Our findings suggest that iron oxide nanoparticles can be tailor-made to possess improved peroxidase-like activity. Such enhancements could further widen nanoparticle scope in glucose detection and extend its peroxidase functionality to other biomedical applications.

Keywords

Superparamagnetic nanoparticle; Iron oxide; Peroxidase; Glucose Detection

Introduction

Magnetic, iron oxide nanoparticles have found in-roads to numerous biomedical applications including magnetic resonance imaging (MRI) [1]; magnetic targeting and drug delivery [2];

[*]Correspondence and reprint requests should be addressed to: Victor C. Yang, Ph.D., Albert B. Prescott Professor of Pharmaceutical Sciences, College of Pharmacy, University of Michigan, 428 Church Street, Ann Arbor, Michigan 48109-1065, Tel: (734) 764-4273; Fax: (734) 763-9772, vcyang@umich.edu.

protein isolation and purification [3]; and magnetic hyperthermia [4]. Recently, it was also reported that iron oxide nanoparticles could function like an artificial peroxidase [5], a finding of great significance. Compared to naturally occurring peroxidase enzymes, nanoparticles are considerably more stable and possess an almost unchanged catalytic activity over a wide range of temperature and pH [5]. Peroxidase enzymes, prone to proteolytic degradation, are difficult to produce in large quantities. In contrast, iron oxide nanoparticles can be readily synthesized in mass yield (via chemical means) and at relatively low cost.

In light of such advantages, nanoparticles could potentially replace peroxidases in various applications, including those dependent on the detection of hydrogen peroxide. For instance, glucose can be monitored indirectly by of the release of hydrogen peroxide following its oxidation by glucose oxidase (GOx) [6, 7]. Immunoenzyme assays [8, 9] are also primarily based on the detection of hydrogen peroxide [10, 11]. Peroxidase catalyzes oxidation of certain substrates to produce characteristic color in the presence of hydrogen peroxide. Such chromogenic reactions have become a powerful tool in analytical detection.

The catalytic power of iron oxide nanoparticles, however, has not been thoroughly explored. Peroxidase-like activity dictates detection sensitivity and, thus, the practical applicability of nanoparticles to function like an enzyme. Clearly, nanoparticles would have little use if activity were too low. When considering factors that might contribute to activity, several questions arise: a) does the structure (e.g. coating, iron oxide content) of the nanoparticle influence its activity? b) is activity related to the structure of substrates? and c) is activity affected by sodium azide, an inhibitor of horseradish peroxidase (HRP) and common preservative used in the storage of biological reagents?

It was reported that peroxidase activity stems from superficial ferrous atoms of nanoparticles[5]. Unfortunately, little improvement in surface ferrous content can be made once nanoparticles are synthesized. Activity, however, might be improved by optimizing affinity toward substrate. A nanoparticle must first form an intermediate complex with its substrate before catalysis can occur. Therefore, a higher affinity to its substrate could lead to a higher catalytic activity.

Affinity may be improved by enhancing electrostatic interaction between substrate and the nanoparticle surface. Two substrates that would be useful to evaluate this hypothesis are 2,2'-azino-bis(3-ethylbenzthiazoline-6-sulfonic acid) diammonium salt (ABTS) and 3,3',5,5'-tetramethylbenzidine (TMB). Both substrates undergo distinguishable color change when enzymatically oxidized with hydrogen peroxide. TMB carries two amine groups, likely yielding stronger affinity toward a negatively charged nanoparticle surface. Conversely, ABTS possesses two sulfonic acid groups, likely exhibiting higher affinity toward a positively charged nanoparticle surface. Therefore, modification of the nanoparticle surface with different charge and charge intensity could enhance (or hinder) observed activity. Modifying nanoparticles with different coatings is one way to alter surface charge.

This work evaluated the impact of surface charge, charge intensity, and coating thickness on the ability of an iron oxide nanoparticle to function as an artificial peroxidase. Our aim was to develop a strategy to synthesize nanoparticles with improved activity and yield higher sensitivity in various biomedical applications. As a model, hydrogen peroxide produced from oxidation of glucose by GOx was measured to indirectly measure glucose.

Materials and methods

Chemicals and reagents

All materials were purchased and used as received without further treatment. Materials used include sodium citrate dehydrate (Fisher Scientific), ferrous chloride tetrahydrate (Fluka), iron chloride hexahydrate (Sigma-Aldrich), carboxymethyl dextran (CMD, 14,400Da, Fluka), polylysine (PLL, 4,000-15,000Da, Sigma-Aldrich), poly(ethyleneimine) (PEI, 10,000Da, Polysciences, Inc), heparin (Sigma), 3,3',5,5'-tetramethylbenzidine, (TMB, KPL), http://en.wikipedia.org/wiki/IUPAC_nomenclature 2,2'-azino-bis(3-ethylbenzthiazoline-6-sulfonic acid) diammonium salt (ABTS, BioChemika), hydrogen peroxide (Sigma-Aldrich), β-D-glucose (TCI America), glucose oxidase (GOx, from *Aspergillus niger*, Sigma), and horseradish peroxidase(HRP, Sigma-Aldrich)

Preparation of iron oxide nanoparticles

Unmodified iron oxide nanoparticles (N_{nat})—Iron oxide nanoparticles were synthesized according to a modified procedure by Kim et al[12]. Briefly, a solution containing 0.76 mol/L of ferric chloride and 0.4 mol/L of ferrous chloride (molar ratio of ferric to ferrous was approximately 2:1) was prepared in pH 1.7 water under nitrogen protection. The iron solution was then added drop-wise to 1.5 mol/L NaOH under vigorous mechanical stirring. This reaction mixture was gradually heated (1°C/min) to 78 °C and held at this temperature for one hour under stirring and nitrogen protection. After separation of the supernatant with a permanent magnet, the wet solid was treated with 0.01 mol/L HCl and then sonicated for 1 hour. The acidified suspension was filtered through 0.45 μm and 0.22 μm membranes. Concentration was then adjusted to 0.7 mg Fe/mL.

Citrate- and glycine-modified iron oxide nanoparticles (N_{cit}, N_{gly})—To 200 mL of 1 mg/mL sodium citrate, 200 mL of 0.7 mg Fe/mL iron oxide nanoparticles were added under stirring. The mixture was sonicated for 20 min and then further stirred for 2 hours. After ultrafiltration to remove free sodium citrate, the concentration was adjusted to 0.35 mg Fe/mL. An analogous procedure was used to obtain glycine-modified nanoparticles (N_{gly}).

Polylysine- and poly(ethyleneimine)-coated iron oxide nanoparticles (N_{PLL}, N_{PEI})—To 100 mL of 1 mg/mL PLL solution, 100 mL of 0.35 mg Fe/mL N_{cit} were added under stirring. The mixture was sonicated for 20 min and then further stirred for 2 hours. The N_{PLL} product was obtained by removing free PLL via ultrafiltration. An analogous procedure was used to obtain PEI-modified nanoparticles (N_{PEI}).

Carboxymethyl dextran- and heparin-coated iron oxide nanoparticles (N_{CMD}, N_{hep}): To 100 mL of 1 mg/mL CMD solution, 100 mL of 0.35 mg Fe/mL N_{gly} were added under stirring. The mixture was sonicated for 20 min and then further stirred for 2 hours. The N_{CMD} product was obtained by removing free CMD via ultrafiltration. An analogous procedure was used to obtain heparin-modified nanoparticles (N_{hep}).

Characterization of synthesized iron oxide nanoparticles

Particle size and zeta potential were measured on a NICOMP 380 ZLS dynamic light scattering (DLS) instrument (PSS, Santa Barbara, CA, USA) equipped with a HeNe laser at 632 nm as the incident light. For size measurements, a volume-weighted distribution was obtained. Zeta potential measurements were taken after nanoparticles were diluted and dispersed with deionized water. High-resolution transmission electron microscopy (HRTEM) was conducted using a JEOL 3011 high-resolution electron microscope (JEOL Tokyo, Japan) operated at an accelerated voltage of 300 kV. Samples were prepared by applying diluted particle suspensions to formvar film-coated copper grids (01813-F, Ted

Pella, Inc, USA) followed by drying preparations at room temperature. A thermogravimetric analyzer (TGA; TA Instruments Q50, New Castle, DE, USA) calibrated with nickel and alumel standards was employed to determine coating content of nanoparticles. Samples were analyzed in a nitrogen atmosphere with a heating rate of 20°C/min. Superparamagnetic properties were assessed at 25 °C using a superconducting quantum interference device (SQUID) (Quantum Design Inc., San Diego, CA, USA). Iron content of nanoparticles was measured by inductively coupled plasma-optical emission spectroscopy (ICP-OES) on an Optima 2000 DV instrument (Perkin-Elmer, Inc., Boston, MA, USA). Samples were spiked with yttrium internal standard and calibrated with water dilutions of an iron standard (GFS Chemicals, Columbus, OH). FTIR was performed on lyophilized samples after compression into ~1 mm thick discs containing spectroscopic grade potassium bromide.

Measurement of peroxidase-like activity

In triplicate, 100 μL of 530 mmol/L hydrogen peroxide containing varied concentrations of chromogenic substrate (TMB or ABTS) were added to 50 μL of the different prepared nanoparticles (0.35 mg Fe/mL). The blue (TMB) or green (ABTS) color that developed as reactions proceeded was monitored kinetically at room temperature using a PowerWave X340 spectrophotometer (BioTek, Winooski, VT). TMB conversion was measured at 655 nm and ABTS at 415 nm. Catalytic parameters were determined by fitting the absorbance data to the Michaelis-Menten equation. Activity was also evaluated in the presence of varied concentrations (0–0.08 wt %) of sodium azide. HRP was also tested for comparison purposes.

Glucose detection

40 μL of 10 mg/mL GOx was added to 200 μL of glucose at varied concentrations in 10 mmol/L phosphate buffered saline (PBS, pH 7.4) and incubated at 37 °C for 30 min. 360 μL of 4.0 mmol/L ABTS and 400 μL of 0.13 mg Fe/mL nanoparticles (both in 0.2 mol/L acetate buffer, pH 4.0) were then added to the oxidized glucose solution above and incubated at 45 °C for 45 min. The reaction mixture was then subject to centrifugation at 15,000 rpm for 10 min to remove nanoparticulate material. 300 μL of the supernatant was analyzed at 417 nm to determine ABTS conversion. Control experiments were conducted using blank (no glucose) PBS.

Results

Synthesis and characterization of iron oxide nanoparticles

FTIR spectra of N_{cit} and N_{gly} show a peak at 1402cm^{-1}, which was not found on the spectra of N_{nat} (Figure 1). This peak was assigned to the Fe-O-C(O) linkage [13], indicating chemical adsorption of citrate/glycine carboxylate groups onto superficial iron atoms found on the nanoparticle surface. Unbound carboxylate groups render N_{cit} negatively charged, whereas unbound amine groups result in a positively charged N_{gly}. Taking advantage of these surface charges, N_{PLL} and N_{PEI} were prepared by electrostatic coating of N_{cit} with positively charged PLL or PEI, respectively. Analogously, N_{CMD} and N_{hep} were synthesized by coating N_{gly} with negatively charged CMD or heparin. Zeta potential results shown in Table 1 show that iron oxide nanoparticles with different coatings – three anionic (N_{cit}, N_{CMD}, N_{hep}) and three cationic (N_{gly}, N_{PLL}, N_{PEI}) –were successfully synthesized. N_{hep} yielded the highest negative zeta potential of −51.2 mV whereas N_{PEI} showed the highest positive zeta potential of +47.1 mV.

Size measurements by DLS showed that all synthesized nanoparticles possessed similar diameters in the range of 35–46 nm (shown in Table 1), indicating that size would not be a confounding variable in subsequent experiments. Moreover, the relative thickness of coating

can be determined by weight loss estimated in a TGA analysis. TGA analyses of N_{PLL}, N_{CMD}, $N_{PEI,}$ and N_{hep} show relatively high weight losses (see Table 1 and Figure 2), corresponding to thicker coatings. Conversely, TGA revealed a relatively low weight loss for N_{cit} and N_{gly} (and thinner coating) due to the size of the small molecules, glycine and citrate. Additionally, HRTEM images in Figure 3 provide visual confirmation that polymer coating of the nanoparticles was successfully achieved. All tested nanoparticles were found to exhibit superparamagnetic behavior (i.e. no hysteresis in demagnetization curves) when examined by SQUID (Figure 4), rendering them suitable for magnetic-mediated, biomedical applications. Coating processes did not appear to alter the magnetic properties of these nanoparticles. Overall, findings consistently support the notion that desired nanoparticles were obtained as designed. In addition, our surface modification procedures for nanoparticles were much simpler than methods described in the literature [14]. Processes were also highly consistent and reproducible. More importantly, no aggregation of nanoparticles was observed for any of the coating processes, and the recovery yield was almost 100%.

Surface charge dependence on peroxidase activity

The peroxidase-like behavior of the synthesized nanoparticles was examined at room temperature using either TMB or ABTS as a chromogenic substrate. Absorbance data was back-calculated to concentration by the Beer-Lambert Law using a molar absorption coefficient of 39000 $M^{-1}cm^{-1}$ for TMB- [15] or 36000 $M^{-1}cm^{-1}$ for ABTS-derived [16] oxidation products. Apparent steady-state reaction rates at different concentrations of substrate were obtained by calculating the slopes of initial absorbance changes with time. Data shown in Figure 5 indicate that all nanoparticles displayed hyperbolic kinetics, yet curve characteristics varied with the type of coating. Data were fit to the Michaelis-Menten equation (curves shown in Figure 5) and model parameters (V_{max} and K_M) extracted. The catalytic constant (k_{cat}; V_{max} normalized for enzyme content) was also calculated according to Equation 1:

$$k_{cat}=V_{max}/[E] \quad (1)$$

where [E] was taken as the nanoparticle iron concentration. Catalytic parameters for each of the nanoparticles tested are summarized in Table 2.

Figure 6 illustrates the dependency of peroxidase activity on superficial charge. ABTS catalysis (curve A) increased rapidly with increasing zeta potential. In a less dramatic fashion, TMB catalysis (curve B) decreased with increasing zeta potential. Indeed, the nanoparticle with the strongest negative surface charge (N_{hep}) exhibited a 5.9-fold higher peroxidase activity than that with the most positive (N_{PEI}) when TMB was the substrate. Conversely, N_{PEI} displayed an 11.5-fold increase in catalytic activity over N_{hep} when ABTS was the substrate.

Coating thickness dependence on peroxidase activity

The effect of coating thickness on peroxidase activity was also studied. The pairs N_{cit}/N_{CMD} and N_{gly}/N_{PLL} served to meet this purpose. The pair N_{cit}/N_{CMD} had similar negative surface charge (shown in Table 1), allowing for controlled comparison of the effect of coating thickness on activity. N_{cit} exhibited a higher k_{cat} than N_{CMD} with both TMB and ABTS substrates (Table 2). Because N_{CMD} has a thicker coating than N_{cit}, steric effects might account for its lower activity for both substrates. As expected, N_{gly} displayed a higher k_{cat} than that of the similarly charged N_{PLL} with TMB as the substrate. Interestingly, the k_{cat} of N_{gly} was lower than that of N_{PLL} with ABTS as the substrate. Although this finding appears

contradictory to the observed trends for thickness, competition between thickness and charge effects might explain this discrepancy. N_{PLL} did have a slightly higher positive zeta potential than N_{gly}. ABTS catalysis was favored by a higher positive surface charge (Figure 6). Hence, a slightly higher positive charge would have greater effect on activity than a thicker coating, as suggested by the steep curve (A) observed for ABTS in Figure 6. It should be noted that neither N_{PEI} nor N_{hep} was included in the above comparison because both nanoparticles exhibited distinct zeta potentials from other samples tested.

Effect of sodium azide on peroxidase activity

Experimental results with sodium azide are shown in Figure 7. The presence of sodium azide resulted in significantly greater loss of activity with HRP when compared to any of the evaluated nanoparticles. For instance, when sodium azide concentration increased to 0.02% (typical for bacteriostatic storage), HRP lost over 99% of its activity. In sharp contrast, tested nanoparticles retained at least 93% activity at the same concentration of sodium azide. In fact, nanoparticles remained relatively active even with a four-fold increase in sodium azide concentration (0.08%). As shown in Figure 7, between 54–82% of activity remained depending on the coating. Retained activity, even in the presence of high sodium azide concentration, further suggests that iron oxide nanoparticles are durable and might be useful in environments where peroxidases (like HRP) can significantly lose function.

Glucose detection by iron oxide nanoparticles

Glucose content could be readily detected by utilizing the same chromogenic substrates studied above. In principle, hydrogen peroxide evolved from GOx oxidation of glucose can oxidize ABTS in the presence of a peroxidase. The color change from converted ABTS can be used to indirectly measure glucose. Based on the findings above, it was thought that N_{PEI} would yield the highest sensitivity among the tested nanoparticles, since it yielded the highest activity toward ABTS. Unfortunately, intense precipitation occurred when N_{PEI} was exposed to glucose/GOx. To this regard, N_{gly}, which also possessed favorable activity toward ABTS (Table 2), was used as a substitute. For comparison, the least active nanoparticle, N_{hep}, was also examined.

Sensitivity results are presented in Figure 8. As shown, absorbance linearly correlated to glucose concentration for both N_{gly} and N_{hep}. The absorbance, though, gradually leveled off and even decreased after glucose concentration exceeded 500 μmol/L (data not shown). Nevertheless, linear ranges of these two types of nanoparticles varied in their slopes, a prime indicator of sensitivity toward glucose. A higher slope would represent a higher sensitivity to glucose. The higher slope for N_{gly} predicts the same absorbance value at a lower glucose concentration when compared to the shallower curve for N_{hep}. Indeed, N_{gly} displayed a slope of 1.251 as opposed to 0.910 from N_{hep} (Figure 8A).

At very low concentrations, N_{gly} still demonstrated good linearity toward glucose (R^2 = 0.993), as shown in Figure 8B. N_{hep}, however, lost some of its linearity as evidenced by a much lower correlation (R^2 = 0.771). This result shows that N_{hep} is unable to provide a linear response to glucose in such a low range of concentrations. The detection limits for N_{gly} and N_{hep}, calculated as three times background absorbance divided by the corresponding line slopes, were estimated to be 8.5 μmol/L and 15.8 μmol/L, respectively. Our data indicate that N_{gly} is more sensitive than N_{hep} when ABTS is chosen as a substrate to detect glucose.

Discussion

Functionalizing iron oxide nanoparticles usually involves a complicated, multistep process that often results in precipitation. In this study, a facile and efficient methodology was established. Iron oxide nanoparticles with six different coatings—three anionic (N_{cit}, N_{CMD}, N_{hep}) and three cationic (N_{gly}, N_{PLL}, N_{PEI})—were synthesized and evaluated to determine the effect of surface charge on peroxidase-like activity. In addition, nanoparticle pairs—having similar charge but different coating thickness— were assessed to understand the effect of coating thickness on peroxidase activity. Of important note, we planned to use N_{nat} as a control in experiments. N_{nat}, though, were unstable at the experimental conditions utilized, quickly precipitating when tested. Therefore, they were not included in analyses.

To prepare nanoparticles with different coatings, N_{cit} and N_{gly} were used as parent materials. Citrate was chemically linked to superficial iron atoms on N_{nat} via its carboxylate groups. The remaining residual carboxylate groups render N_{cit} negatively charged [17, 18]. The aminated nanoparticle, N_{gly}, was synthesized analogously. Since the carboxylate group of glycine bound to nanoparticles as those from citrate, free glycine amino group rendered a net positive surface charge for N_{gly}. To our knowledge, this strategy has not yet been applied to synthesize an aminated nanoparticle. Based on our observations, our methodology is far simpler, more reproducible, and most importantly, without nanoparticle aggregation.

Highly branched PEI consists of primary, secondary, and tertiary amine groups in an approximate 25/50/25 ratio according to information from the manufacturer. PLL has an abundance of lysine groups that contain amine moieties. PEI and PLL can both be anchored to the surface of N_{cit} via electrostatic interactions between amine groups on the polymer and free carboxylate groups of N_{cit}. In a similar fashion, N_{CMD} and N_{hep} were prepared by electrostatically coating N_{gly} with CMD or heparin, respectively. CMD provides free carboxylate and heparin provides both free carboxylate and sulfate groups that can bind free amine groups on N_{gly}. Characterization of these nanoparticles confirmed that coatings were successfully achieved as designed.

Previous results [5] indicate that superficial ferrous atoms are a contributing factor to observed peroxidase activity. Structure-wise, a large area-to-volume ratio (characteristic of a small particle size) would favor an enhanced catalytic activity. In this work, a group of iron oxide nanoparticles was prepared, all with similar size. Size was carefully controlled in order to keep it from confounding experiments. It is also important to mention that catalytic constants were expressed in terms of iron atom instead of particle number. If constants were calculated in terms of particle number, a large particle would yield a larger catalytic constant because of its larger surface area – the source of catalytic activity. Catalytic constants based on mass or atom number, though, provide a more normalized basis by which to evaluate activity.

Michaelis-Menten kinetics can be described by Equation 2:

$$E+S \underset{k_{-1}}{\overset{k_1}{\longleftrightarrow}} ES \xrightarrow{k_2} E+P \tag{2}$$

According to Equation 2, increasing k_1 and decreasing k_{-1} could improve enzyme activity. One route to do so would be to enhance affinity between enzyme and substrate. To achieve this purpose, electrostatic interaction appeared to be the simplest and most efficient strategy, as our results support. ABTS and TMB were chosen because they possess opposite charge characteristics. ABTS contains negatively charged sulfonic groups, giving it a strong electrostatic affinity toward a positively charged nanoparticle. As our results demonstrate,

such an enhanced affinity results in a significantly improved peroxidase activity. Conversely, TMB contains two amine groups, yielding a strong affinity toward a negatively charged nanoparticle. Analogous to the reaction between ABTS and a positively charged nanoparticle, an anionic nanoparticle will exhibit a strong affinity and high activity with TMB as the reaction substrate. Experimental data were in strong support of these claims, as demonstrated by the calculated catalytic parameters shown in Table 2.

The Michaelis constant (K_M) is an indicator of enzyme affinity for its substrate. A high K_M represents a weak affinity whereas a low value suggests a high affinity [19]. In Table 2, this relationship is clearly illustrated. Cationic nanoparticles yielded lower K_M values toward negatively charged ABTS, and the opposite occurred for TMB as the substrate. Therefore, the rationale for varied activity was that affinity was altered by changes in electrostatic interaction between particle and substrate. Moreover, the intensity of superficial charge on nanoparticles appeared to also influence the degree to which catalytic activity was altered, as peroxidase activity varied with varied zeta potential (Figure 6). Among the nanoparticles studied, N_{hep} had the highest negative charge and N_{PEI} the highest positive charge. In support of our claim, N_{hep} showed the highest activity with TMB and the lowest with ABTS as the substrate. Conversely, N_{PEI} showed the highest activity with ABTS and the lowest with TMB as the substrate (see Figure 6).

Although electrostatic affinity exerted by superficial charge could enhance catalytic activity, the physical presence of a coating could also shield active iron domains on the surface of particles. This effect was observed when comparing particles of similar charge, but different coating thickness. As noted, however, steric effects on affinity were relatively weak compared with the dramatic changes seen with varied zeta potentials.

A common challenge to the application of peroxidases (such as HRP) lies in their easy inactivation by standard antibacterial preservatives, such as sodium azide [20]. The catalytic turnover of sodium azide by peroxidase into azidyl radical results in peroxidase inactivation [20]. Inactivation cripples the applicability of peroxidases in applications. Nanoparticles, regardless of superficial charge or the coating, however, exhibited robust resistance against sodium azide. Activity of nanoparticles was virtually unaffected by the presence of sodium azide, especially at commonly utilized concentrations. To this regard, iron oxide nanoparticles offer a durable alternative to peroxidases by their ability to function even in harsh environments detrimental to protein enzymes.

The utility and applicability of the synthesized nanoparticles was further demonstrated through their sensitivity and detection limit in glucose measurements. Compared with N_{hep}, N_{gly} displayed a larger linear slope of ABTS absorbance with glucose concentrations, suggesting better sensitivity for glucose detection. In addition, a better linear correlation was observed in the low concentration range, suggesting an improved detection limit. The low detection limit observed for N_{gly} could be useful to applications that measure low levels of glucose. For example, it was reported that the glucose concentration in tear fluid is correlated to that in the blood [21, 22]. An accurate analysis of glucose in tear fluid could be a viable, noninvasive alternative for diabetes mellitus patients. The glucose concentration in tear fluid is relatively low (~28μmol/L) [22] and more than 100-fold less than in blood. Our data suggest that an iron oxide nanoparticle might be a good candidate to assay glucose in tears, or in other applications that require analysis of trace levels of glucose. Excellent sensitivity, detection limit, and linearity in our model glucose assay support the use of iron oxide nanoparticles in other quantitative assays dependent on peroxidase activity.

Conclusion

The peroxidase-like activity of iron oxide nanoparticles was explored and found dependent on the surface attributes of nanoparticles. Six nanoparticles were synthesized with distinct surface charge, charge intensity, and coating thickness. With TMB as a substrate, anionic nanoparticles had a high affinity and exhibited a high catalytic activity. The activity gradually decreased when varying the zeta potential from negative to positive. N_{hep} exhibited a 5.9-fold higher catalytic activity than N_{PEI}. With ABTS as the substrate, cationic nanoparticles displayed a high affinity and subsequently a high peroxidase activity. The activity increased dramatically in varying the zeta potential from negative to positive. N_{PEI} displayed an 11.5-fold higher activity than N_{hep}. The intrinsic peroxidase activity of these nanoparticles was virtually unaffected by the presence of standard antibacterial preservative of sodium azide. Particles yielding a high activity toward an ABTS as a substrate, such as N_{gly}, exhibited a much higher sensitivity and a much lower limit in glucose detection than N_{hep}, a particle of low catalytic activity.

Acknowledgments

This research was in part supported by NIH grants CA114612 and RNS066945 as well as a Hartwell Biomedical Research Award. Dr. Faquan Yu is a recipient of the Hubei Natural Science Fund for Distinguished Young Scholars (2005ABB031), Hubei, China. Mr. Adam Cole is the recipient of an NIH Pharmacological Sciences and Bio-related Chemistry Training Program grant (GM007767 from NIGMS) and of an American Foundation of Pharmaceutical Education (AFPE) Pre-Doctoral Fellowship. Dr. Victor Yang is currently a Cheung Kong Scholar appointed by Chinese Ministry of Education.

References

1. Lewin M, Carlesso N, Tung CH, Tang XW, Cory D, Scadden DT, et al. Tat peptide-derivatized magnetic nanoparticles allow in vivo tracking and recovery of progenitor cells. Nat Biotechnol. 2000; 18(4):410–414. [PubMed: 10748521]
2. Cheng J, Teply BA, Jeong SY, Yim CH, Ho D, Sherifi I, et al. Magnetically responsive polymeric microparticles for oral delivery of protein drugs. Pharm Res. 2006; 23(3):557–564. [PubMed: 16388405]
3. Hancock JP, Kemshead JT. A rapid and highly selective approach to cell separations using an immunomagnetic colloid. J Immunol Methods. 1993; 164(1):51–60. [PubMed: 7689621]
4. Matteucci ML, Anyarambhatla G, Rosner G, Azuma C, Fisher PE, Dewhirst MW, et al. Hyperthermia increases accumulation of technetium-99m-labeled liposomes in feline sarcomas. Clin Cancer Res. 2000; 6(9):3748–3755. [PubMed: 10999769]
5. Gao L, Zhuang J, Nie L, Zhang J, Zhang Y, Gu N, et al. Intrinsic peroxidase-like activity of ferromagnetic nanoparticles. Nat Nanotechnol. 2007; 2(9):577–583. [PubMed: 18654371]
6. Geschke, O.; Klank, H.; Telleman, P. Microsystem Engineering of Lab-on-a-chip Devices. Wiley-VCH Verlag GmbH & Co. KGaA; 2004. p. 220
7. Jin Z, Chen R, Colon LA. Determination of glucose in submicroliter samples by CE-LIF using precolumn or on-column enzymatic reactions. Anal Chem. 1997; 69(7):1326–1331. [PubMed: 21639340]
8. Boorsma DM, Van Bommel J, Vanden Heuvel J. Avidin-HRP conjugates in biotin-avidin immunoenzyme cytochemistry. Histochem Cell Biol. 1986; 84(4–6):333–337.
9. Dhawan S. Signal amplification systems in immunoassays: implications for clinical diagnostics. Expert Rev Mol Diagn. 2006; 6(5):749–760. [PubMed: 17009908]
10. El-Essi FA, Zuhri AZA, Al-Khalil SI, Abdel-Latif MS. Spectrophotometric determination of enzymatically generated hydrogen peroxide using Sol-Gel immobilized horseradish peroxidase. Talanta. 1997; 44(11):2051–2058. [PubMed: 18966952]
11. Fernandes KF, Lima CS, Lopes FM, Collins CH. Hydrogen peroxide detection system consisting of chemically immobilised peroxidase and spectrometer. Process Biochem. 2005; 40(11):3441–3445.

12. Kim DK, Zhang Y, Voit W, Rao KV, Muhammed M. Synthesis and characterization of surfactant-coated superparamagnetic monodispersed iron oxide nanoparticles. J Magn Magn Mater. 2001; 225(1–2):30–36.

13. Yu S, Chow GM. Carboxyl group (-CO_2H) functionalized ferrimagnetic iron oxide nanoparticles for potential bio-applications. J Mater Chem. 2004; 14(18):2781–2786.

14. Sun EY, Josephson L, Kelly KA, Weissleder R. Development of nNanoparticle libraries for biosensing. Bioconjugate Chem. 2006; 17(1):109–113.

15. Karaseva EI, Losev YP, Metelitsa DI. Peroxidase-catalyzed oxidation of 3,3″,5,5″-tetramethylbenzidine in the presence of 2,4-dinitrosoresorcinol and polydisulfide derivatives of resorcinol and 2,4-dinitrosoresorcinol. Russ J Bioorg Chem. 2002; 28(2):128–135.

16. Forni LG, Mora-Arellano VO, Packer JE, Willson RL. Nitrogen dioxide and related free radicals: electron-transfer reactions with organic compounds in solutions containing nitrite or nitrate. J Chem Soc, Perkin Trans II. 1986; 2:1–6.

17. Bacri J-C, Perzynski R, Salin D, Cabuil V, Massart R. Ionic ferrofluids: A crossing of chemistry and physics. J Magn Magn Mater. 1990; 85(1–3):27–32.

18. Fauconnier N, Bee A, Massart R, Dardoize F. Direct determination of organic acids in a ferrofluid (γ-Fe_2O_3) by high-Performance liquid chromatography. J Liq Chromatogr Relat Technol. 1996; 19(5):783–797.

19. Berg, JM.; Tymoczko, JL.; Stryer, L. Biochemistry. 6. New York: W. H. Freeman; 2007. p. 221

20. Brill AS, Weinryb I. Reactions of horseradish peroxidase with azide. evidence for a methionine residue at the active site. Biochemistry. 1967; 6(11):3528–3535. [PubMed: 6073036]

21. Giardini A, Roberts JRE. Concentration of glucose and total chloride in tears. Br J Ophthalmol. 1950; 34(12):737–743. [PubMed: 14821266]

22. Baca JT, Taormina CR, Feingold E, Finegold DN, Grabowski JJ, Asher SA. Mass spectral determination of fasting tear glucose concentrations in nondiabetic volunteers. Clinic Chem. 2007; 53(7):1370–1372.

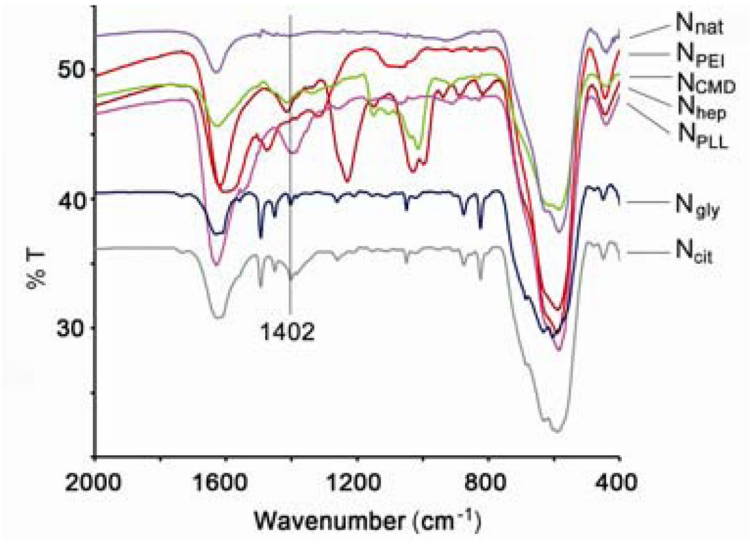

Figure 1.

FTIR spectra of the synthesized nanoparticles. FTIR spectra of both N_{cit} and N_{gly} showed a new peak at 1402cm^{-1}, which corresponds to symmetric stretching of Fe-O-C(O) bonds. This band confirms successful coating. As a comparison, N_{nat} (no coating) showed no such peak.

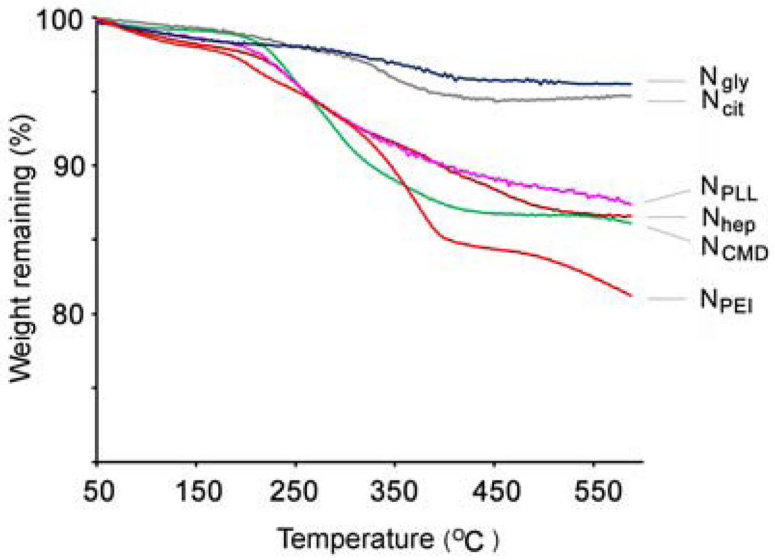

Figure 2.

TGA analyses of the synthesized nanoparticles. TGA of polymer-coated particles (N_{PLL}, N_{CMD} N_{hep} and N_{PEI}) displayed a higher weight loss than small-molecule-coated particles (N_{cit} and N_{gly}). Heating rate was controlled at 20°C/min in a nitrogen atmosphere. Higher weight losses suggest relatively thicker coatings.

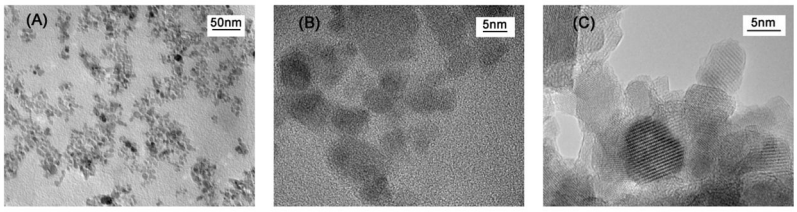

Figure 3.

TEM images of (a) N_{PLL} on a copper grid coated with a continuous formvar film at lower magnification. Nanoparticles are clearly well dispersed. (b) N_{PLL} on a copper grid coated with a continuous formvar film at higher magnification. A shell-type coating can be observed on nanoparticles. The coating, however, is hard to see due to interference from the carbon film background; (c) N_{PLL} on a copper grid coated with a lacey network support film to minimize background interference, yielding higher resolution. The image better demonstrates the core/shell structure of N_{PLL}.

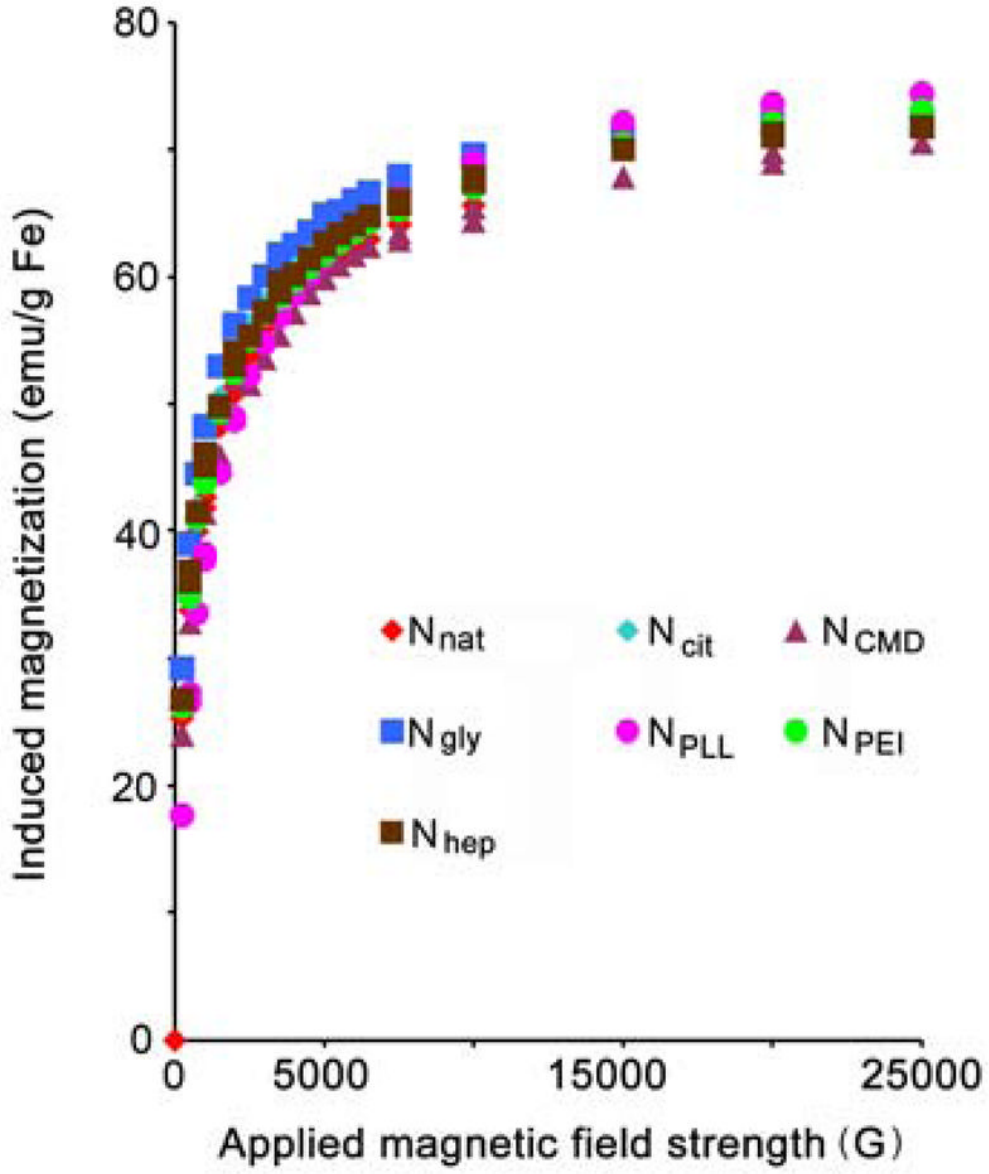

Figure 4.
SQUID magnetization/demagnetization curves of the six different nanoparticle products. The lack of hysteresis in demagnetization curves demonstrates superparamagnetic behavior of the nanoparticle products.

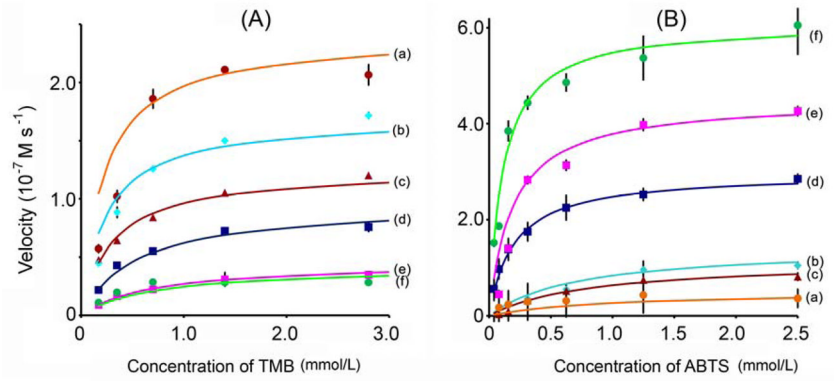

Figure 5.

Kinetic analyses of (a) N_{hep}, (b) N_{cit}, (c) N_{CMD}, (d) N_{gly}, (e) N_{PLL}, and (f) N_{PEI}. Steady-state catalysis rates were calculated from the initial slopes of absorbance versus time curves. Experiments were conducted by adding 50 μL of nanoparticle suspensions (0.35 mg Fe/mL) into solutions containing 100 μL of 530 mmol/L H_2O_2 and different concentrations of (A) TMB; and (B) ABTS substrate at room temperature. Points represent experimental data and color curves correspond to calculated fits using the Michaelis-Menten model.

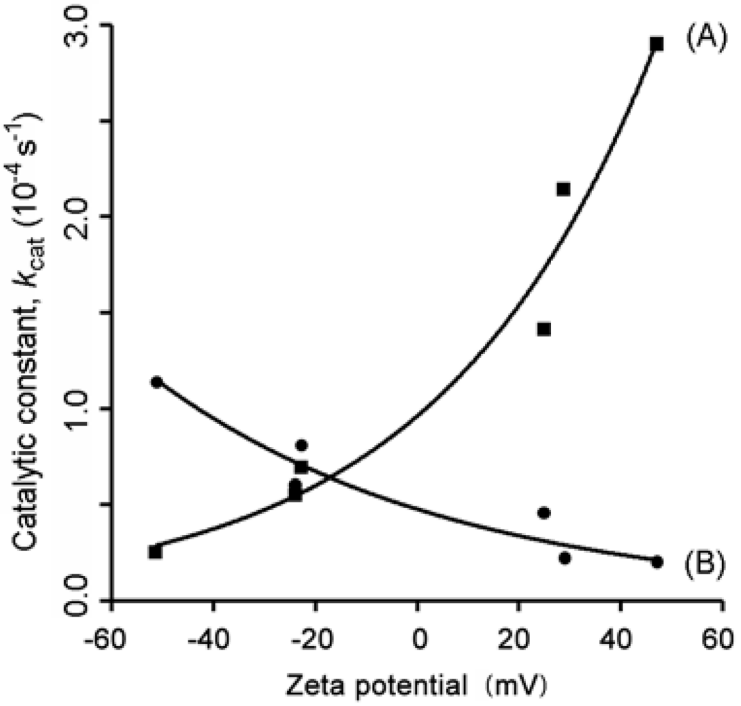

Figure 6.

Plots of catalytic constant (k_{cat}) versus zeta potential for the different nanoparticle products, with ABTS (Curve A) or TMB (Curve B) as the substrate. Zeta potentials were derived from Table 1. For an ABTS substrate, k_{cat} increases rapidly with increasing zeta potential. In a much less pronounced manner, k_{cat} decreases with increasing zeta potential for a TMB substrate.

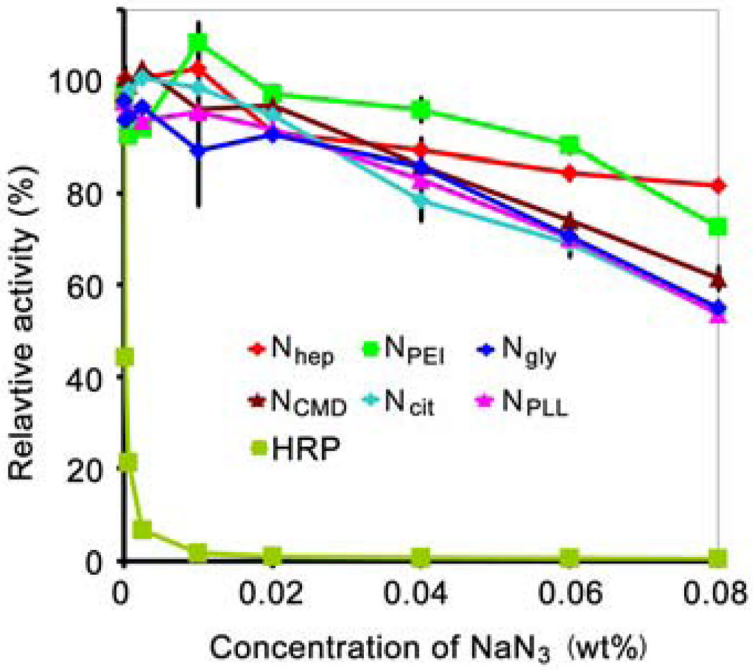

Figure 7.

Inhibition of peroxidase activity by azide for the different nanoparticle products. For comparison, horseradish peroxidase (HRP) was tested. As shown, all products tested retained relatively high activity even at high azide concentrations. Conversely, almost all peroxidase activity was lost when HRP was exposed to even small levels of azide.

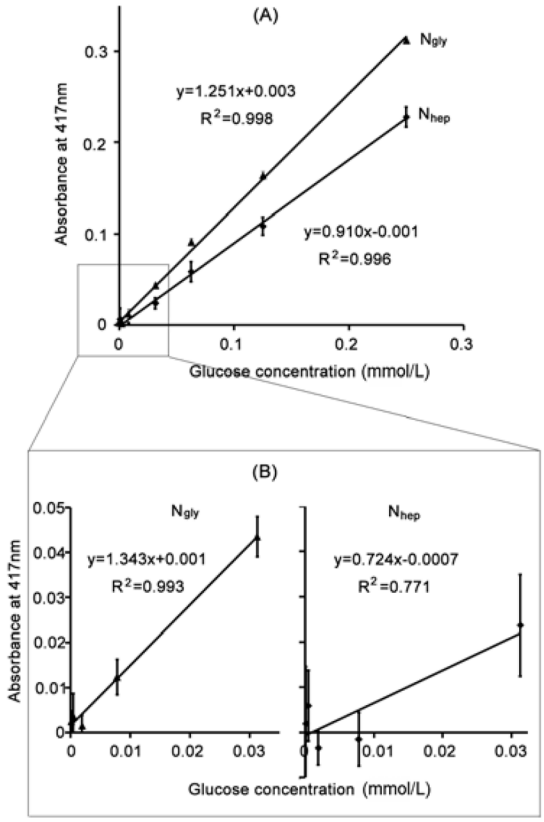

Figure 8.

Glucose detection using N_{gly} and N_{hep} (ABTS substrate). Response curves for N_{gly} and N_{hep} at (A) high; and (B) low (i.e. <31.2 μmol/L) glucose concentrations are shown. N_{gly} showed higher sensitivity when compared to N_{hep} as evidenced by a higher slope. Where N_{hep} lost its linearity in the low glucose concentration range shown (B), N_{gly} retained it across both ranges tested suggesting a better detection limit.

Table 1

Properties of iron oxide nanoparticles with different coatings

Nanoparticle	Coating material	Size by DLS, (nm)	Weight % of coating shell by TGA	Zeta potential, (mV)
N_{cit}	citrate	34.4	2.0	−22.7
N_{CMD}	CMD	42.1	12.1	−23.8
N_{hep}	heparin	40.6	13.5	−51.2
N_{gly}	glycine	40.1	1.6	+25.0
N_{PLL}	PLL	46.2	10.5	+28.9
N_{PEI}	PEI	43.7	18.7	+47.1

CMD: carboxymethyl dextran, PLL: polylysine, PEI: poly(ethyleneimine)

Table 2

Michaelis-Menten parameters of tested nanoparticles

Nanoparticle	TMB			ABTS		
	K_M (mmol/L)	V_{max} (10^{-7}Ms^{-1})	k_{cat}[a] (10^{-4}s^{-1})	K_M (mmol/L)	V_{max} (10^{-7}Ms^{-1})	k_{cat}[a] (10^{-4}s^{-1})
N_{cit}	0.24	1.70	0.81	0.73	1.45	0.69
N_{CMD}	0.30	1.25	0.60	0.81	1.15	0.55
N_{hep}	0.22	2.40	1.14	0.96	0.52	0.25
N_{gly}	0.55	0.96	0.46	0.20	2.97	1.41
N_{PLL}	0.69	0.46	0.22	0.19	4.50	2.14
N_{PEI}	0.71	0.42	0.20	0.12	6.10	2.90

[a]Catalytic constant derived from $k_{cat}=V_{max}/[E]$, where V_{max} is the maximum reaction rate reached with increasing TMB or ABTS concentration, as shown in Figure 5; [E] is the nanoparticle iron concentration measured by inductively coupled plasma-optical emission spectroscopy (ICP-OES).